

Supporting Information

Ceria promoted Co@NC catalyst for biofuel upgrade: synergy between ceria and cobalt species

Bowei Wang^{abc}, Ruixiao Gao^a, Dan Zhang^a, Yuyao Zeng^a, Fangying Zhang^a, Xilong Yan^{abc}, Yang Li^{abc*}, Ligong Chen^{abc*}

^a School of Chemical Engineering and Technology, Tianjin University, Tianjin 300350, P. R. China.

^b Collaborative Innovation Center of Chemical Science and Engineering (Tianjin), Tianjin 300072, P. R. China.

^c Tianjin Engineering Research Center of Functional Fine Chemicals, Tianjin, P. R. China.

* Corresponding authors. E-mail: lgchen@tju.edu.cn (L. Chen); liyang777@tju.edu.cn (Y. Li)

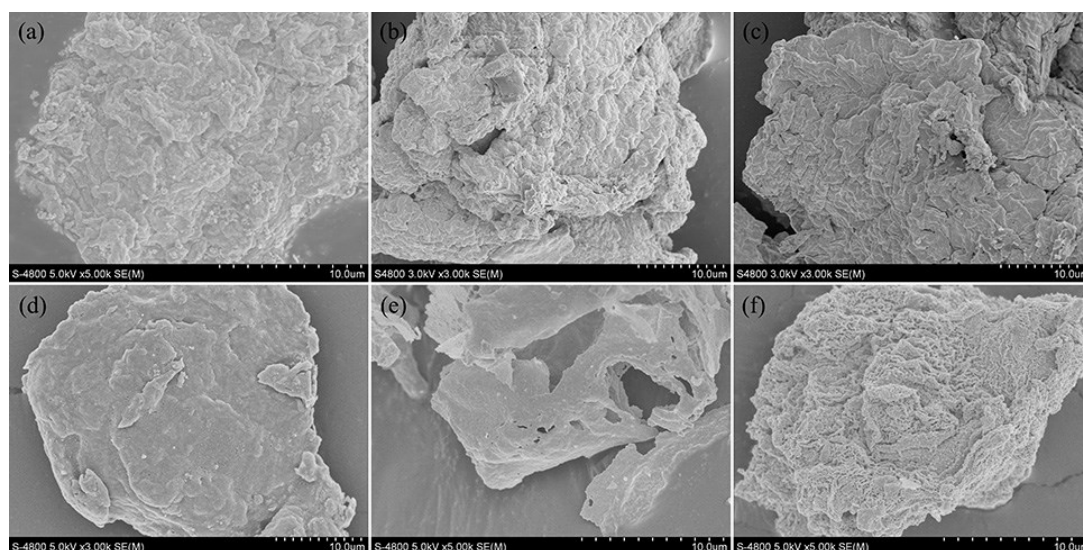


Fig. S1. SEM images of (a) Co/Ce@NC-700, (b) Co/Ce@NC, (c) Co/Ce@NC-1000, (d) Co@NC, (e) Co/Ce, and (f) Ce@NC.

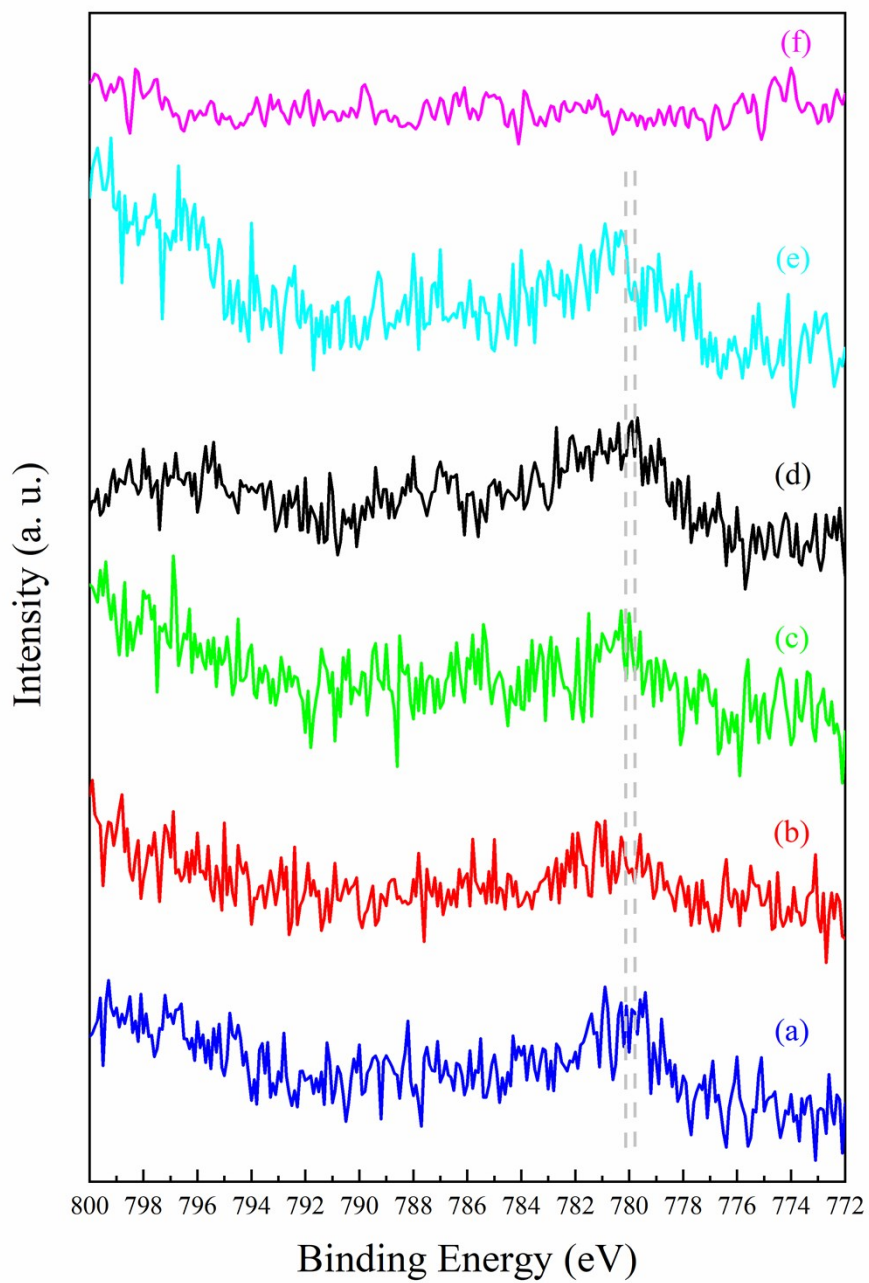


Fig. S2. High-resolution XPS spectra of Co 2p region for (a) Co/Ce@NC-700, (b) Co/Ce@NC, (c) Co/Ce@NC-1000, (d) Co@NC, (e) Co/Ce, and (f) Ce@NC.

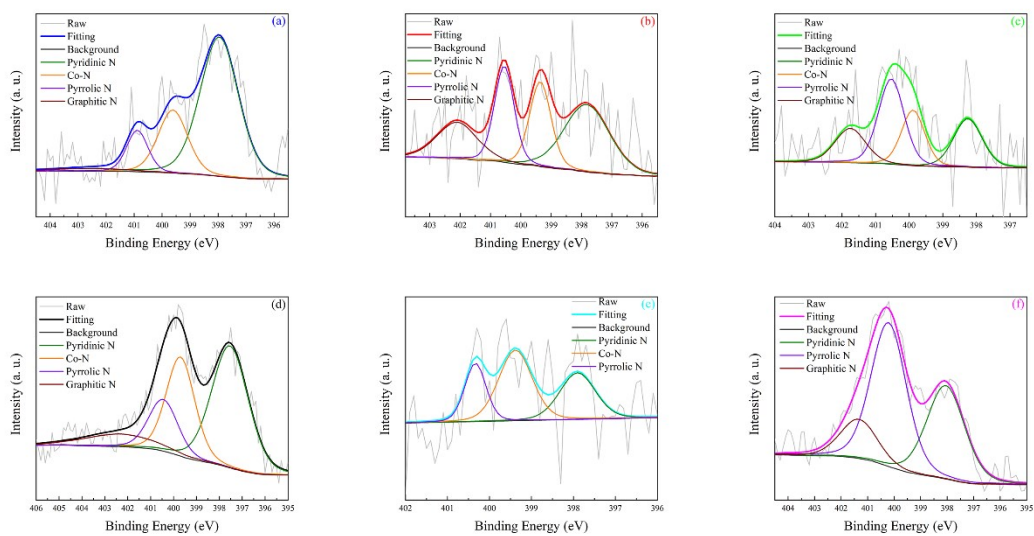


Fig. S3. High-resolution XPS spectra of N 1s region for (a) Co/Ce@NC-700, (b) Co/Ce@NC, (c) Co/Ce@NC-1000, (d) Co@NC, (e) Co/Ce, and (f) Ce@NC.

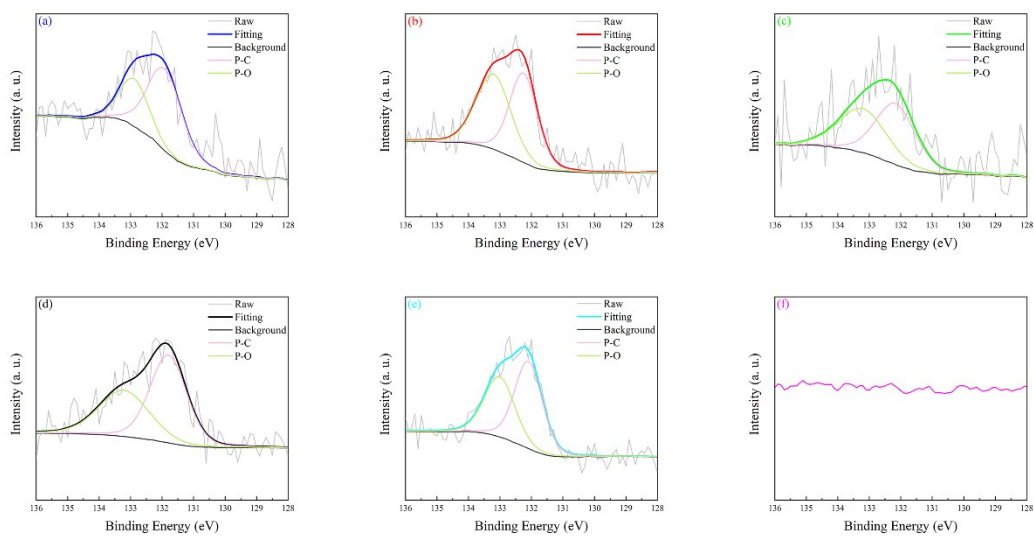


Fig. S4. High-resolution XPS spectra of P 2p region for (a) Co/Ce@NC-700, (b) Co/Ce@NC, (c) Co/Ce@NC-1000, (d) Co@NC, (e) Co/Ce, and (f) Ce@NC.

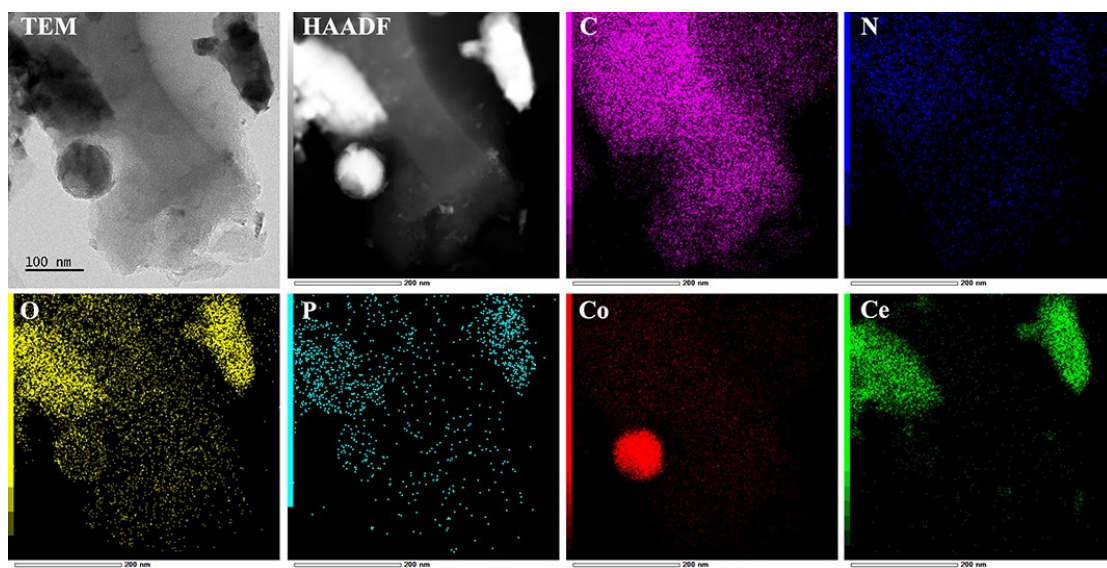


Fig. S5. TEM, HAADF, and EDS mapping images of Co-CeO₂@NC.

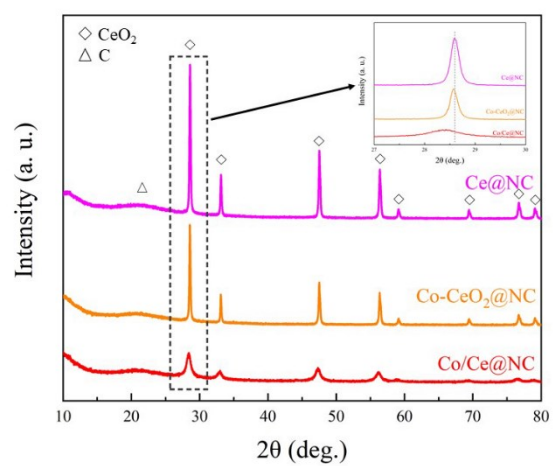


Fig. S6. XRD patterns of Co/Ce@NC, Co-CeO₂@NC, and Ce@NC.

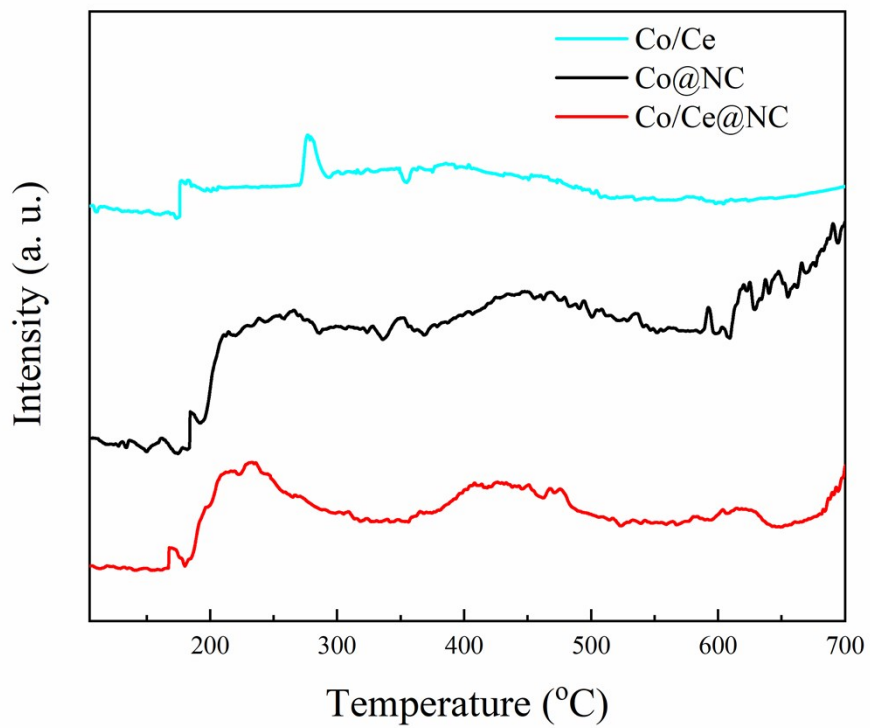


Fig. S7. NH₃-TPD profiles of Co/Ce@NC, Co@NC, and Co/Ce.

Computational methods ^{S13-15}

All static calculations were carried out using spin-polarized density functional theory (DFT) with generalized gradient approximation (GGA) of Perdew-Burke-Ernzerhof (PBE) as implemented in VASP 5.4.4. The cutoff energy of plane-wave basis set is 400 eV and 3 3 1 K-points grid sampling was used for Brillouin zone integration. Atomic positions were optimized by conjugate gradient algorithm until the forces were less than 0.03 eV/Å. Transition states were searched by climbing image nudged elastic-band method (CI-NEB) and further confirmed by vibrational frequency analysis.

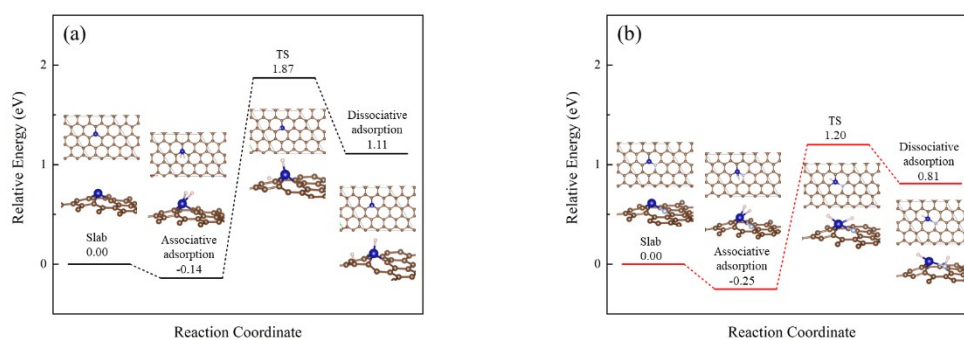


Fig. S8. Relative energy diagram of catalytic H₂ dissociation over Co-loaded graphene without nitrogen species (a) and with pyridine nitrogen species (b).

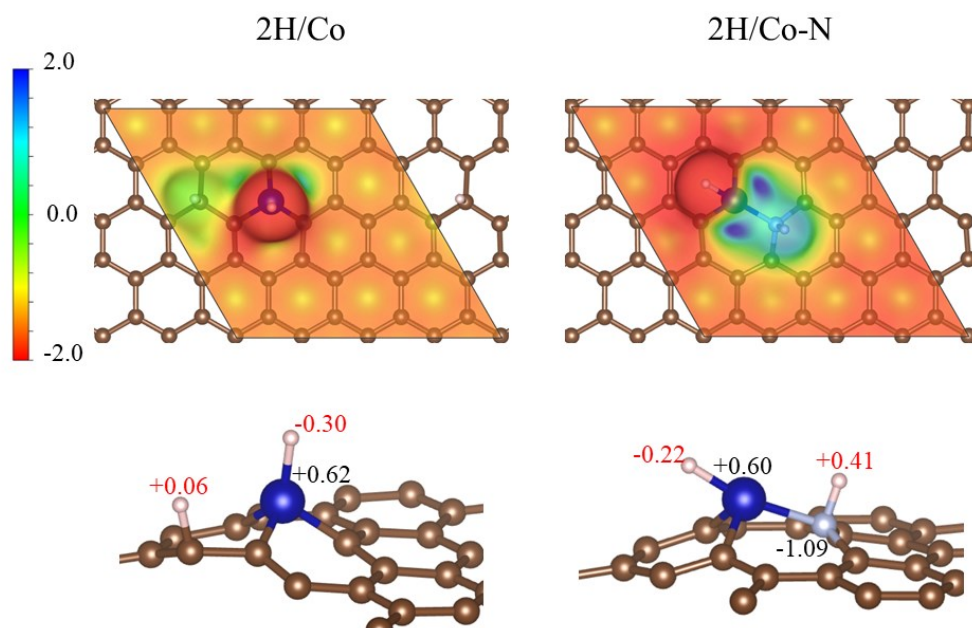


Fig. S9. Electron-density isosurfaces of 2H/Co and 2H/Co-N. The electron-density isosurfaces are plotted at $0.005 \text{ e} \cdot \text{bohr}^{-1}$. The color bar represents the electrostatic potential scale.

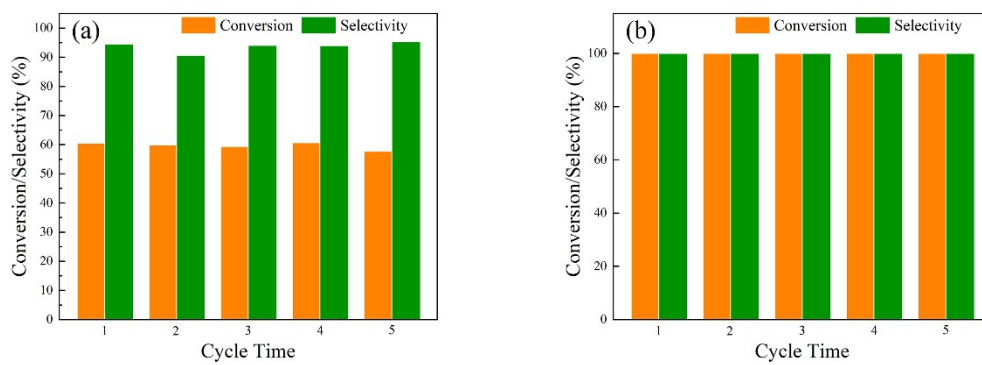


Fig. S10. Stability of Co/Ce@NC. Reaction conditions: vanillin (0.13 mmol); 2 mL ethanol; 5 mol% catalyst; 170 °C; 1 MPa H₂; 3 h (a) or 6 h (b).

Table S1. Summarization for preparation details of catalysts in this work.

Sample ^a	Active metal source	Carbon source	Additive (Source)	Pyrolysis temperature
Co/Ce@NC	vitamin B ₁₂	chitosan	CeO ₂ (Ce(NO ₃) ₃ ·6H ₂ O, 0.63 g)	850 °C
Co/Ce@NC-700	vitamin B ₁₂	chitosan	CeO ₂ (Ce(NO ₃) ₃ ·6H ₂ O, 0.63 g)	700 °C
Co/Ce@NC-1000	vitamin B ₁₂	chitosan	CeO ₂ (Ce(NO ₃) ₃ ·6H ₂ O, 0.63 g)	1000 °C
Co/Ce@C	vitamin B ₁₂	glucose	CeO ₂ (Ce(NO ₃) ₃ ·6H ₂ O, 0.63 g)	850 °C
Co/Ce@NC (WP)	Co(CH ₃ COO) ₂ ·4H ₂ O	chitosan	CeO ₂ (Ce(NO ₃) ₃ ·6H ₂ O, 0.63 g)	850 °C
Co/Ce	vitamin B ₁₂	-	CeO ₂ (Ce(NO ₃) ₃ ·6H ₂ O, 1.26 g)	850 °C
Co-CeO ₂ @NC	vitamin B ₁₂	chitosan	CeO ₂ (CeO ₂)	850 °C
Ce@NC	-	chitosan	CeO ₂ (Ce(NO ₃) ₃ ·6H ₂ O, 0.63 g)	850 °C
Co@NC	vitamin B ₁₂	chitosan (2.5 g)	-	850 °C
Co@C	vitamin B ₁₂	glucose (2.5 g)	-	850 °C
Fe/Ce@NC	Fe(CH ₃ COO) ₂ ·4H ₂ O	chitosan	CeO ₂ (Ce(NO ₃) ₃ ·6H ₂ O, 0.63 g)	850 °C
Cu/Ce@NC	Cu(CH ₃ COO) ₂ ·H ₂ O	chitosan	CeO ₂ (Ce(NO ₃) ₃ ·6H ₂ O, 0.63 g)	850 °C
Ni/Ce@NC	Ni(CH ₃ COO) ₂ ·4H ₂ O	chitosan	CeO ₂ (Ce(NO ₃) ₃ ·6H ₂ O, 0.63 g)	850 °C
Co/Al@NC	vitamin B ₁₂	chitosan	Al ₂ O ₃ (Al(NO ₃) ₃ ·9H ₂ O, 1.84 g)	850 °C
Co/Si@NC	vitamin B ₁₂	chitosan	SiO ₂ (nano-SiO ₂ , 20 nm)	850 °C
Co/Ti@NC	vitamin B ₁₂	chitosan	TiO ₂ (nano-TiO ₂ , 20 nm)	850 °C

^a General preparation procedure: Initially, the suspension of active metal source (active metal 0.13 mmol), additive (0.25 g), and carbon source (1.25 g) in 80 vol% ethanol (60 mL) was stirred under refluxing for 4 h. Subsequently, the solvent was slowly removed under vacuum. The obtained solid was dried in vacuum at 60 °C and then grounded into a fine powder. Finally, the powder was pyrolyzed at 850 °C for 2 h under argon atmosphere to yield the catalyst.

Table S2. Surface N content, peak positions and relative amount of nitrogen species for Co/Ce@NC-700, Co/Ce@NC, Co/Ce@NC-1000, Co@NC, Co/Ce, and Ce@NC based on XPS analysis

Sample	Surface N Content (wt%)	Pyridinic N		Co-N		Pyrrolic N		Graphitic N	
		BE (eV)	Ratio (%)	BE (eV)	Ratio (%)	BE (eV)	Ratio (%)	BE (eV)	Ratio (%)
Co/Ce@NC-700	4.18	398.0	64.49	399.6	22.50	400.9	10.62	402.5	2.39
Co/Ce@NC	2.50	397.8	37.19	399.4	22.08	400.5	22.97	402.1	17.76
Co/Ce@NC-1000	1.51	398.3	23.32	399.9	21.92	400.5	36.97	401.8	17.79
Co@NC	3.56	397.5	46.02	399.7	29.18	400.5	15.56	402.3	9.24
Co/Ce	1.31	397.9	31.55	399.4	44.91	400.3	23.54	-	-
Ce@NC	3.71	398.1	35.18	-	-	400.2	50.50	401.3	14.32

Table S3. Catalytic hydrogenation of nitrobenzene or styrene

Entry	Catalyst	Substrate	Conversion (%)	Selectivity (%)
1 ^a	Co@NC	nitrobenzene	6.18±0.8	>99 ^c
2 ^a	Co/Ce@NC	nitrobenzene	85.78±1.3	>99 ^c
3 ^b	Co@NC	styrene	62.66±1.0	>99 ^d
4 ^b	Co/Ce@NC	styrene	96.14±1.7	>99 ^d

^a Reaction Conditions: nitrobenzene (0.25 mmol); solvent: methanol (2.50 mL); 0.60 mol% catalyst; 140 °C; 2 MPa H₂; 1 h.

^b Reaction Conditions: styrene (0.13 mmol); solvent: methanol (2.50 mL); 1.20 mol% catalyst; 140 °C; 2 MPa H₂; 4 h.

^c Selectivity of aniline.

^d Selectivity of ethylbenzene.

Table S4. Summary of catalyst consumption among reported non-noble metal-based catalysts for the HDO of vanillin.

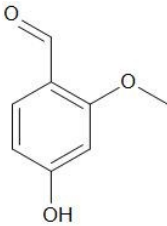
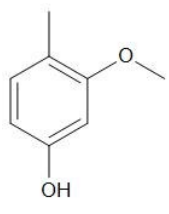
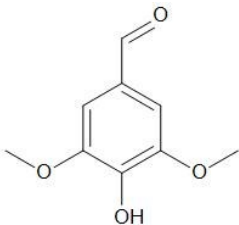
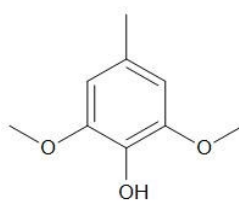
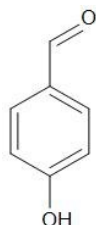

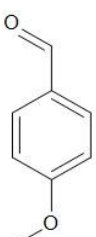
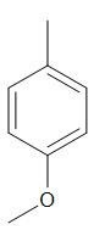
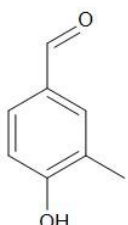
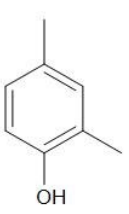
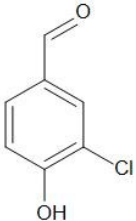
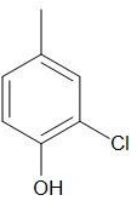
	Catalyst	Catalyst dosage ^a	Hydrogen Source	Solvent	Conv. (%) ^b	Selec. (%) ^c	Ref.
M@NC catalysts	Co/N-C-600	11.82 mol%	H ₂	isopropanol	98.2	85.1	S1
	ZnO/Co-N-CNT	21.48 mol%	H ₂	water	100	89.1	S2
	Co/NG ₈ /CF	19.42 mol%	H ₂	water	95	>99	S3
	Co@NC-700	7.90 mol%	HCOOH	water	95.7	100	S4
	Co@NG-6	4.60 mol%	HCOOH	water	98.5	100	S5
	Co/Ce@NC	5.00 mol%	H ₂	water or ethanol	>99	>99	This
			10.00 mol%	ethanol	ethanol	>99	>99
Other non-noble metal-based catalysts	sulfided CoMo/Al ₂ O ₃	not given	H ₂	dodecane	53	23	S6
	Co _x P@POP	8.26 mol%	H ₂	isopropanol	99.3	83.4	S7
	Ni/NCB-900	2.18 mol%	H ₂	water	74.4	64.6	S8
	SS-Ni/SiO ₂	25.92 mol%	H ₂	decalin	99.8	89.0	S9
	Cu-PMO	11.41 mol%	H ₂	methanol	100	90	S10
	Ga-doped Cu/HNZY	5.10 mol%	H ₂	methanol	100	99	S11
	Cu/AC-600	13.61 mol%	H ₂	water	99.9	93.2	S12
			isopropanol	isopropanol	99.8	99.1	

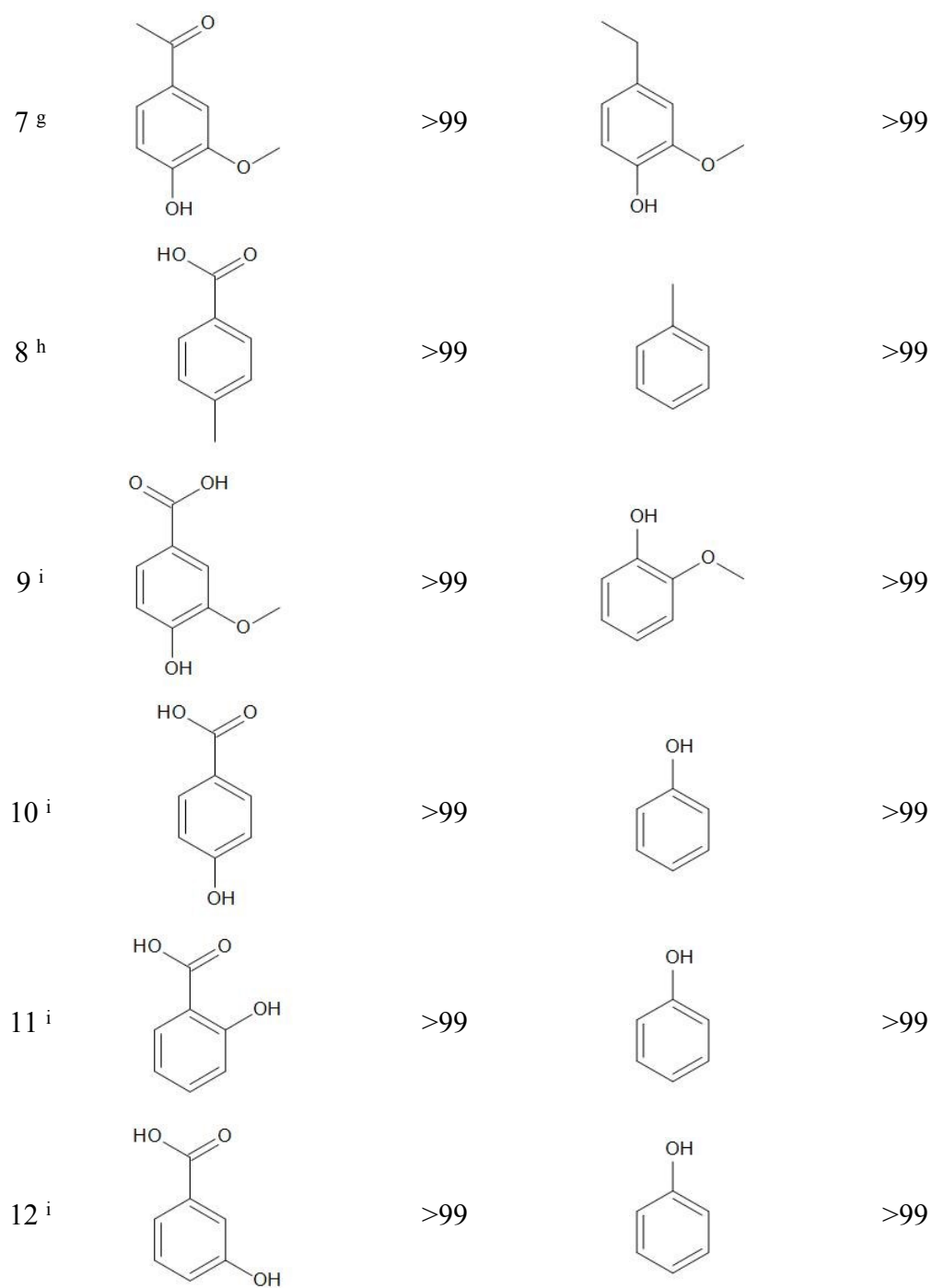
^a based on active metal component.

^b Conversion of vanillin.

^c Selectivity of creosol.

Table S5. General applicability of Co/Ce@NC for hydrodeoxygenation. ^a

Entry	Substrate	Conversion (%)	Product	Selectivity (%)
1 ^b		>99		>99
2 ^c		>99		>99
3 ^d		98.07		>99
4 ^d		98.40		>99
5 ^e		95.74		88.87
6 ^f		97.43		92.00



^a Reaction conditions: substrate (0.13 mmol); 2 mL water; 5 mol% catalyst; 170 °C; 1 MPa H₂. ^b 8 h. ^c 10 h. ^d 12 h. ^e 2 mL ethanol; 22 h. ^f 2 mL ethanol; 18 h. ^g 2 mL ethanol; 24 h. ^h 6 h. ⁱ 4 h.

Table S6. Selection of catalysts ^a

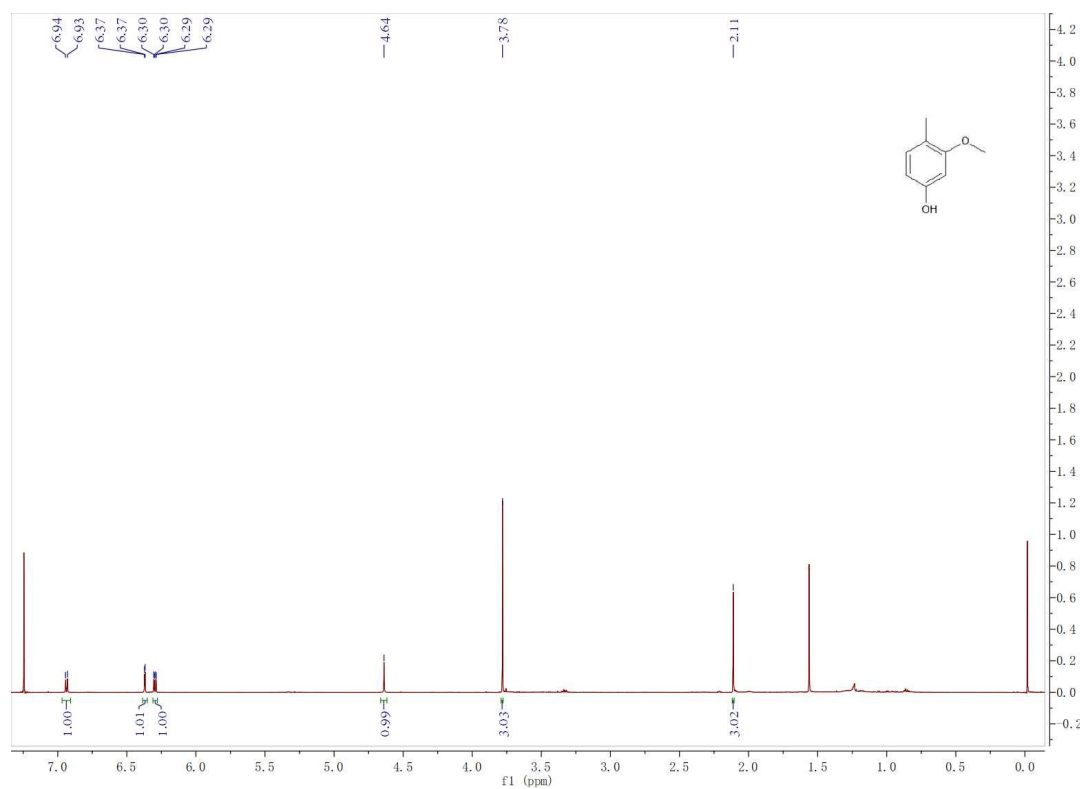
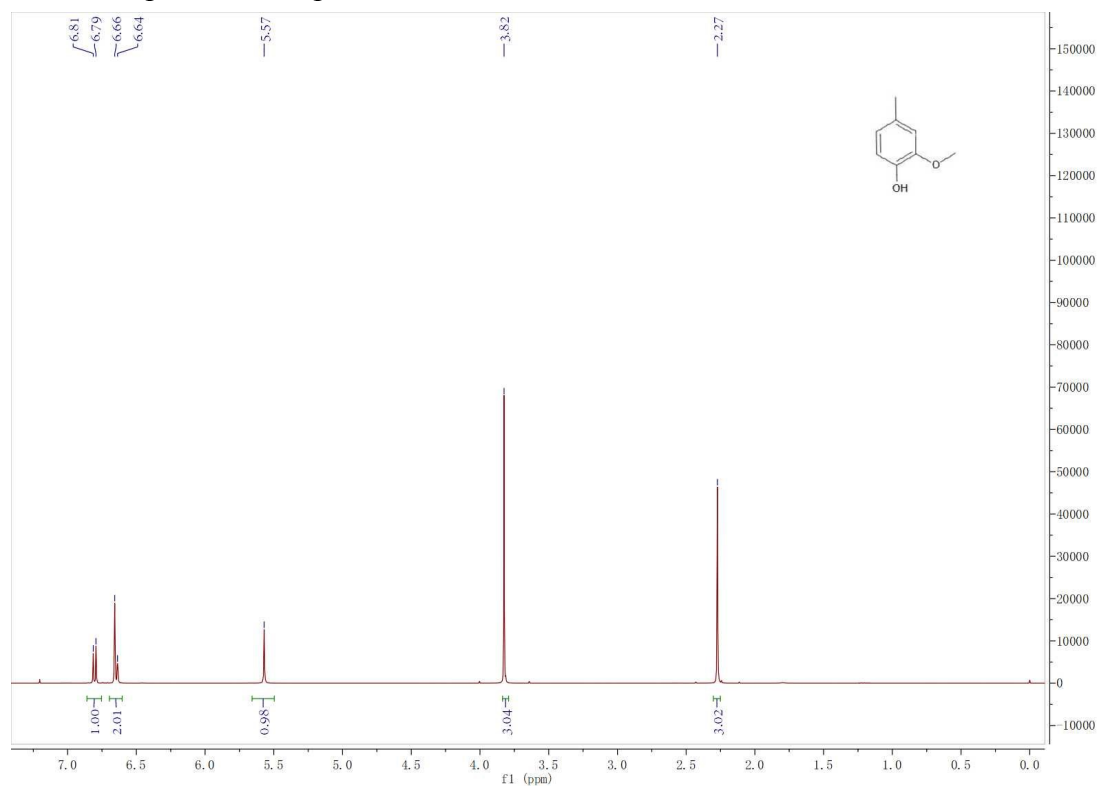
Entry	Catalyst	Conversion (%) ^b	Selectivity (%) ^c
1	Cu/Ce@NC	6.93±0.5	>99
2	Co/Ce@NC	85.78±1.3	>99
3	Ni/Ce@NC	17.8±1.0	>99
4	Fe/Ce@NC	3.38±0.6	>99
5	Co/Al@NC	4.11±0.8	>99
6	Co/Si@NC	29.87±1.0	>99
7	Co/Ti@NC	12.76±1.1	>99

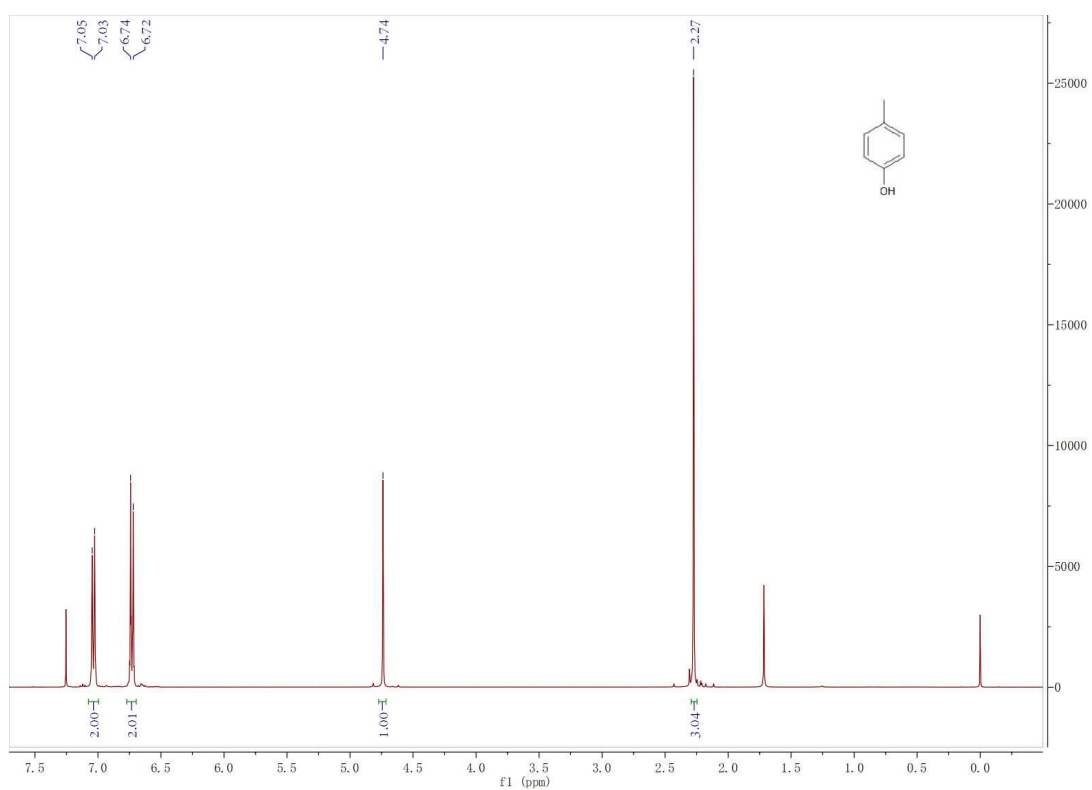
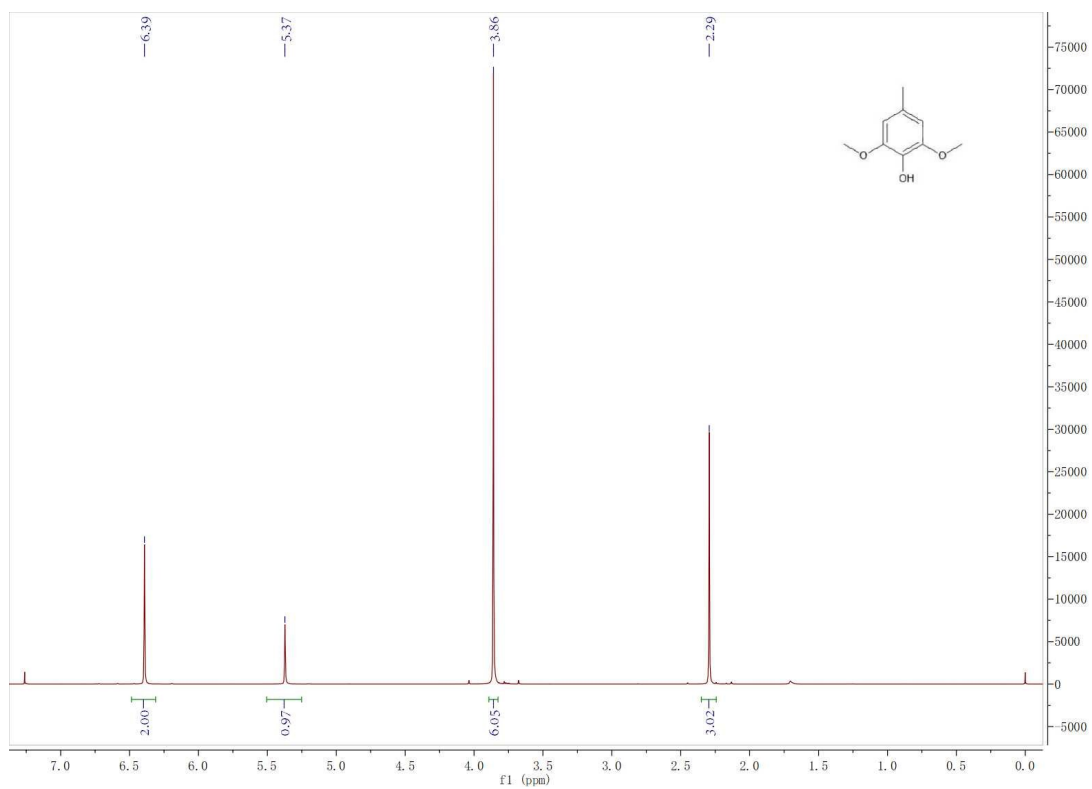
^a Reaction Conditions: nitrobenzene (0.25 mmol); solvent: methanol (2.50 mL); 10 mg catalyst; 140 °C; 2 MPa H₂; 1 h.

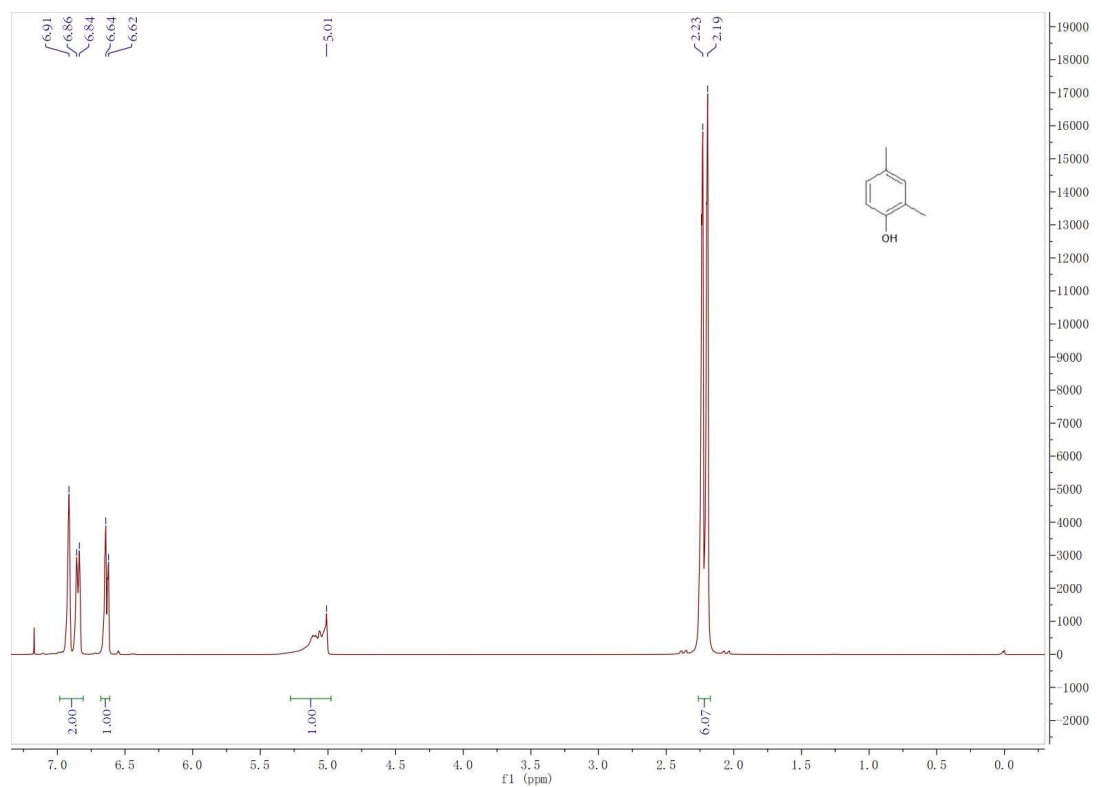
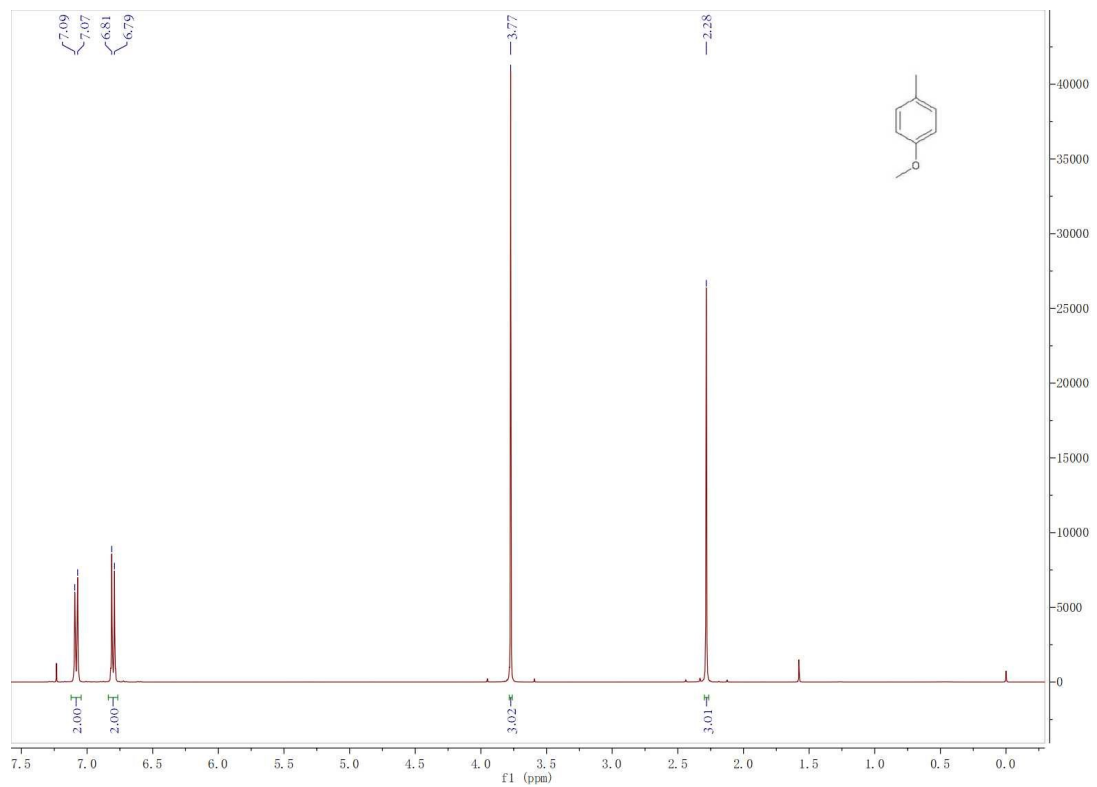
^b Conversion of nitrobenzene.

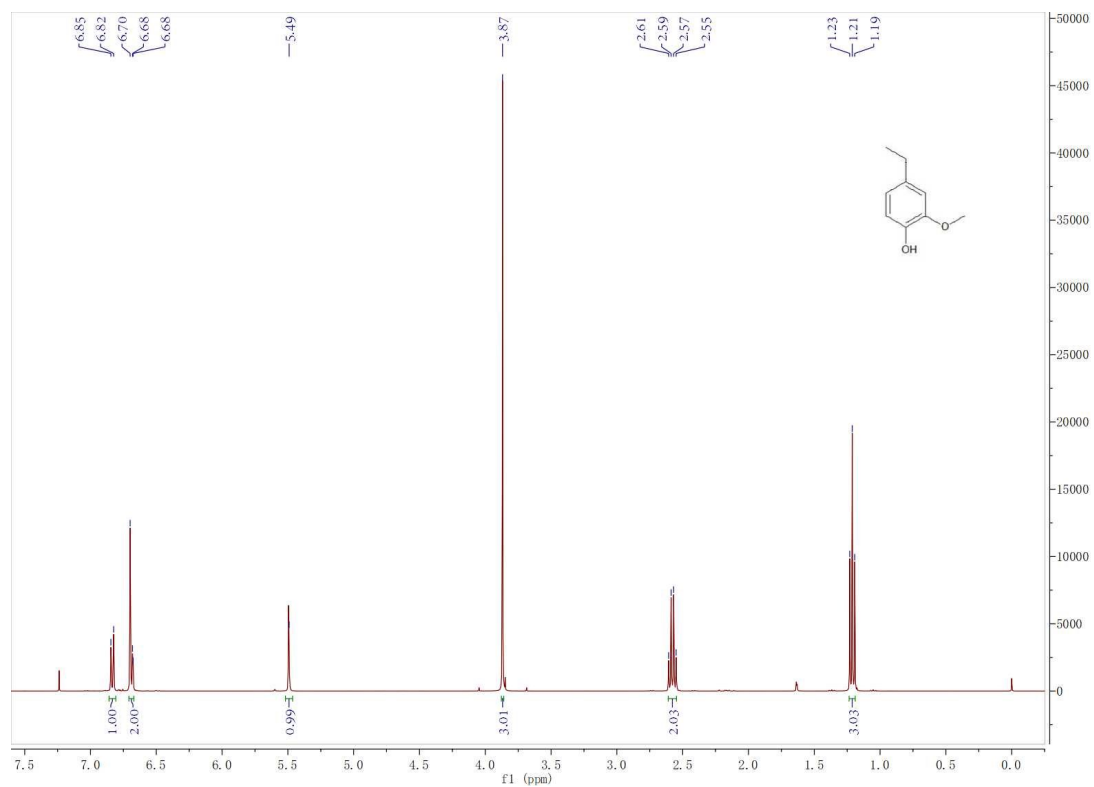
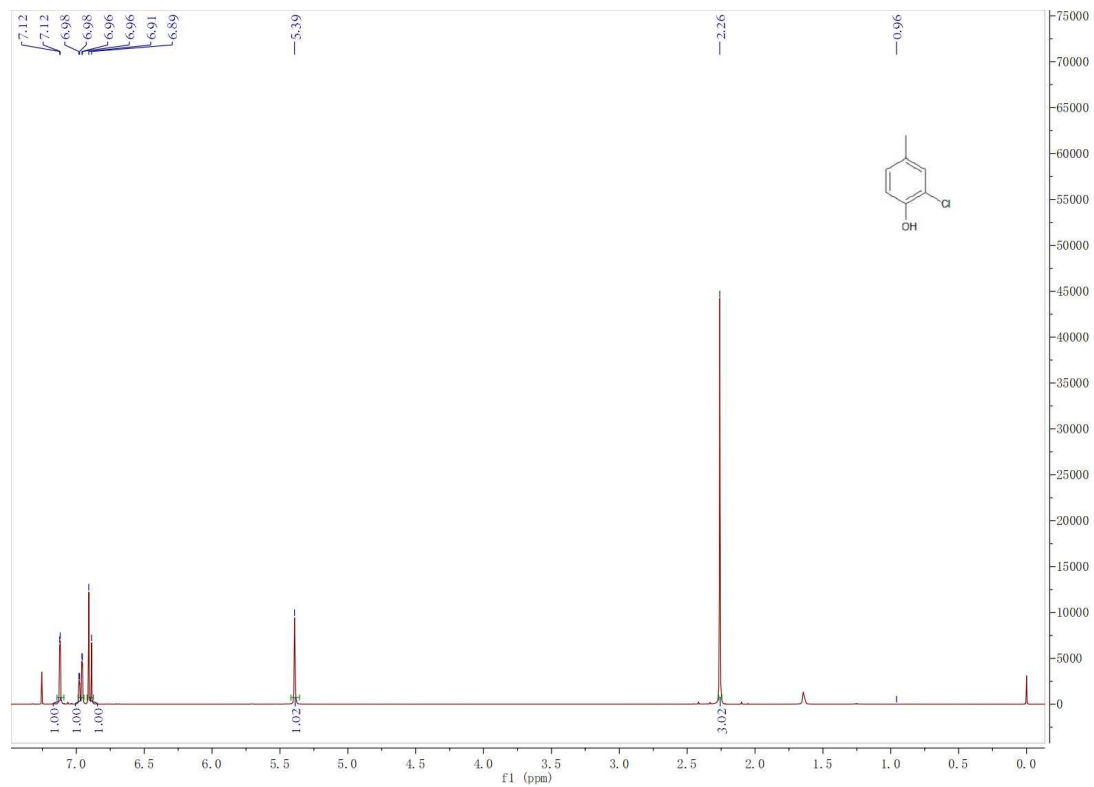
^c Selectivity of aniline.

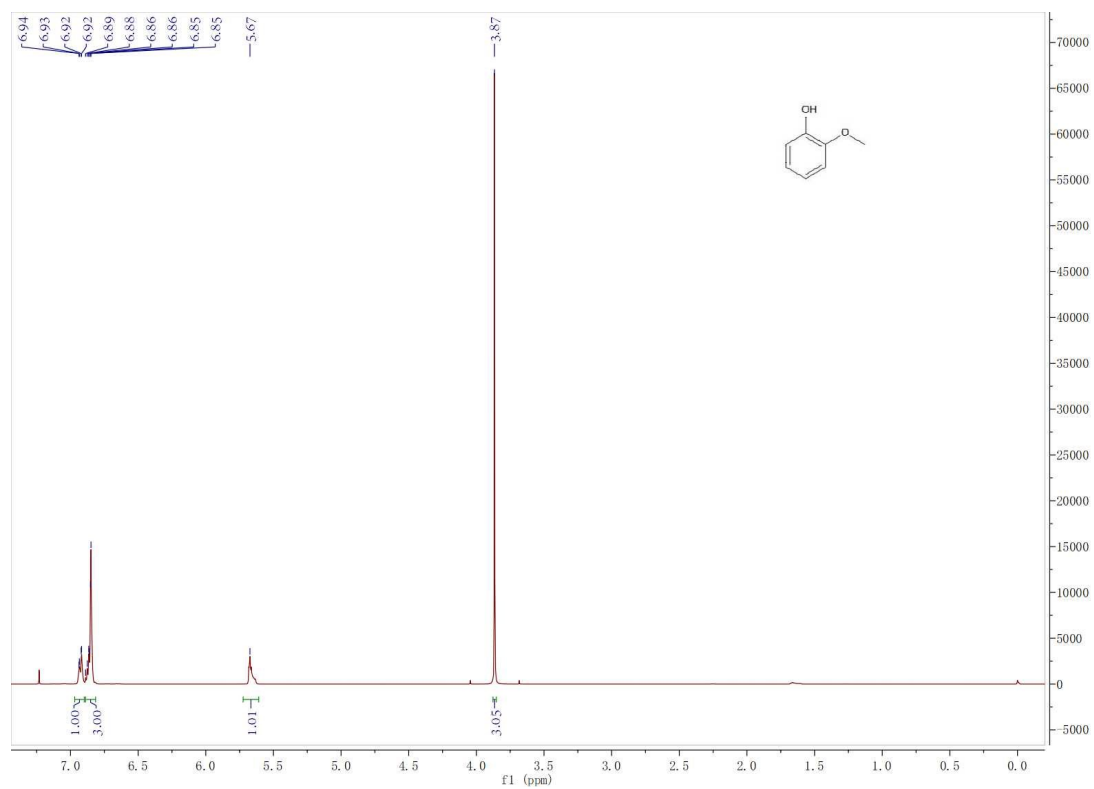
¹H NMR spectra of the products:











References:

- [S1] L. Jiang, P. Zhou, C. Liao, Z. Zhang, S. Jin, *ChemSusChem*, 2018, **11**, 959-964.
- [S2] V. Ranaware, D. Verma, R. Insyani, A. Riaz, S. M. Kim, J. Kim, *Green Chem.*, 2019, **21**, 1021-1042.
- [S3] T. -J. Zhao, J. -J. Zhang, H. -H. Wang, J. Su, X. -H. Li, J. -S. Chen, *ChemSusChem*, 2020, **13**, 1900-1905.
- [S4] H. Yang, R. Nie, W. Xia, X. Yu, D. Jin, X. Lu, D. Zhou, Q. Xia, *Green Chem.*, 2019, **19**, 5714-5722.
- [S5] S. Zhou, F. Dai, C. Dang, M. Wang, D. Liu, F. Lu, H. Qi, *Green Chem.*, 2019, **21**, 4732-4747.
- [S6] A. L. Jongorius, R. Jastrzebski, P. C. A. Bruijninx, B. M. Weckhuysen, *J. Catal.*, 2012, **285**, 315-323.
- [S7] S. C. Shit, P. Koley, B. Joseph, C. Marini, L. Nakka, J. Tardio, *ACS Appl. Mater. Interfaces*, 2019, **11**, 24140-24153.
- [S8] R. Nie, H. Yang, H. Zhang, X. Yu, X. Lu, D. Zhou, Q. Xia, *Green Chem.*, 2017, **19**, 3126-3134.
- [S9] R. Shu, Q. Zhang, Y. Xu, J. Long, L. Ma, T. Wang, P. Chen, Q. Wu, *RSC Adv.*, 2016, **6**, 5214-5222.
- [S10] L. Petitjean, R. Gagne, E. S. Beach, D. Xiao, P. T. Anastas, *Green Chem.*, 2016, **18**, 150-156.
- [S11] D. Verma, R. Insyani, H. S. Cahyadi, J. Park, S. M. Kim, J. M. Cho, J. W. Bae, J. Kim, *Green Chem.*, 2018, **20**, 3253-3270.
- [S12] R. Fan, C. Chen, M. Han, W. Gong, H. Zhang, Y. Zhang, H. Zhao, G. Wang, *Small*, 2018, **14**, 1801953.
- [S13] G. Kresse, J. Furthmüller, *Comput. Mater. Sci.*, 1996, **6**, 15-50.
- [S14] G. Kresse, J. Furthmüller, *Phys. Rev. B*, 1996, **54**, 11169-11186.
- [S15] G. Henkelman, B. P. Uberuaga, H. Jónsson, *J. Chem. Phys.*, 2000, **113**, 9901-9904.